Evaporation of Water Droplets on Polymer Surfaces

ARTICLE *in* LANGMUIR · JUNE 2007

Impact Factor: 4.46 · DOI: 10.1021/la0636309 · Source: PubMed

Evaporation of Water Droplets on Polymer Surfaces

Jung-Hoon Kim,† Sung Il Ahn,† Jae Hyun Kim,‡ and Wang-Cheol Zin*,†

Department of Materials Science and Engineering, Pohang University of Science and Technology, Pohang 790-784, Korea, and Manufacturing Technology Team 1, Memory Division, Semiconductor Business, Samsung Electronics Co., Ltd., San #16 Banwol-Dong, Hwasung-City, Gyeonggi-Do, Korea 445-701

Received December 15, 2006. In Final Form: March 14, 2007

The evaporation of water droplets on polymer surfaces was investigated by using a digital image analysis technique. There were three distinct stages in the water evaporation process: a constant contact area mode, a constant contact angle mode, and a mixed mode that is independent of both the initial quantity of water droplets and the hydrophobic properties of the polymer surfaces. The physical factors influencing the first and second transitions in the evaporation process were found to be the attainment of the receding angle on the polymer surfaces and the Marangoni instability in the evaporating water droplets, which result from the concentration gradient of contaminants. This study also provides qualitative information about the microfluid flows inside the evaporating water droplets and the morphology of drying stains on polymer surfaces. The contaminants were found to be concentrated at the perimeter of the stains, in agreement with the observed outward microfluid flow in the mixed mode of the evaporation process.

Introduction

The evaporation of water droplets is a fundamental phenomenon in nature. Because of its important role in many complex systems such as clouds and fog, the evaporation of water droplets has been a topic of continued interest for several decades.[1−10] In recent years, the formation of a ring of solute on a substrate after the evaporation of a droplet, which is caused by evaporation-driven flow, has become important as a key technique in applications such as DNA/RNA microarrays,[11,12] microlenses,[13] and electronic devices fabricated by the ink-jet printing method.[14−17] Because of these applications, the microfluid flow in evaporating droplets has been theoretically investigated and experimentally visualized.[18−23] The ring of solute on the substrate is produced because the contact line is pinned, so solvent lost by evaporation at the droplet's edge must be replaced by solvent drawn from the center of the droplet. The pinning of the contact line is due to self-pinning, in which the initial roughness or chemical heterogeneities of the substrate provide a foothold on which the contact line sticks; the accumulation of solute at the contact line is then caused by outward microfluid flow from the droplet's center to its edge, which apparently strengthens the pinning, and then eventually takes over as the primary source of pinning.[19]

In the case of a droplet of pure liquid, which does not leave solid components as a result of its drying on a substrate, this process is thought to evolve in two distinct stages: an initial pinned phase in which the base of the droplet stays constant and the contact angle decreases, followed by a second unpinned phase in which the base shrinks but the angle remains fixed because there is no accumulation of solid components at the contact line during the initial pinned phase. To understand these evaporation phenomena, the evaporation of water droplets on mixed self-assembled monolayers has been investigated.[24,25] It was reported in these studies that the difference between the initial contact angle and the average angle in the unpinned phase is consistent with the directly measured wetting hysteresis and the wetting hysteresis is dominated by the roughness rather than by the chemical heterogeneity of the surface. In recent studies, for the second unpinned phase, the inward microfluid flow from the droplet's edge to its center is estimated for contact angles smaller than $\pi/2$ and uniform evaporation.[26,27]

However, it has been reported that droplet evaporation occurs in three distinct stages, as shown in Figure 1.[7,28−31] The first stage is an initial pinned phase (constant contact area mode), the

* Corresponding author. E-mail: wczin@postech.ac.kr. Tel: +82-54-279-2136. Fax: +82-54-279-2399.
† Pohang University of Science and Technology.
‡ Samsung Electronics Co., Ltd.

(1) Picknett, R. G.; Bexon, R. *J. Colloid Interface Sci.* **1977**, *61*, 336.
(2) Birdi, K. S.; Vu, D. T. *J. Phys. Chem.* **1989**, *93*, 3702.
(3) Birdi, K. S.; Vu, D. T. *J. Adhes. Sci. Technol.* **1993**, *7*, 485.
(4) Bourgès-Monnier, C.; Shanahan, M. E. R. *Langmuir* **1995**, *11*, 2820.
(5) Rowan, S. M.; Newton, M. I.; McHale, G. *J. Phys. Chem.* **1995**, *99*, 13268.
(6) Erbil, H. Y.; Meric, R. A. *J. Phys. Chem. B* **1997**, *101*, 6867.
(7) McHale, G.; Rowan, S. M.; Newton, M. I.; Banerjee, M. K. *J. Phys. Chem. B* **1998**, *102*, 1964.
(8) Erbil, H. Y.; McHale, G.; Rowan, S. M.; Newton, M. I. *Langmuir* **1999**, *15*, 7378.
(9) Erbil, H. Y.; McHale, G.; Newton, M. I. *Langmuir* **2002**, *18*, 2636.
(10) Shanahan, M. E. R. *Langmuir* **2002**, *18*, 7763.
(11) Laurell, T.; Nilsson, J.; Marko-Varga, G. *Anal. Chem.* **2005**, *77*, 264A.
(12) Dugas, V.; Broutin, J.; Souteyrand, E. *Langmuir* **2005**, *21*, 9130.
(13) Bonaccurso, E.; Butt, H. -J.; Hankeln, B.; Niesenhaus, B.; Graf, K. *Appl. Phys. Lett.* **2005**, *86*, 124101.
(14) Sirringhaus, H.; Kawase, T.; Friend, R. H.; Shimoda, T.; Inbasekaran, M.; Wu, W.; Woo, E. P. *Science* **2000**, *290*, 2123.
(15) Kawase, T.; Sirringhaus, H.; Friend, R. H.; Shimoda, T. *Adv. Mater.* **2001**, *13*, 1601.
(16) Kawase, T.; Shimoda, T.; Newsome, C.; Sirringhaus, H.; Friend, R. H. *Thin Solid Films* **2003**, *438*−*439*, 279.
(17) Cheng, K.; Yang, M. -H.; Chiu, W. W. W.; Huang, C. -Y.; Chang, J.; Ying, T. -F.; Yang, Y. *Macromol. Rapid Commun.* **2005**, *26*, 247.
(18) Deegan, R. D.; Bakajin, O.; Dupont, T. F.; Huber, G.; Nagel, S. R.; Witten, T. A. *Nature* **1997**, *389*, 829.
(19) Deegan, R. D.; Bakajin, O.; Dupont, T. F.; Huber, G.; Nagel, S. R.; Witten, T. A. *Phys. Rev. E* **2000**, *62*, 756.
(20) Fischer, B. J. *Langmuir* **2002**, *18*, 60.
(21) Hu, H.; Larson, R. G. *Langmuir* **2005**, *21*, 3963.
(22) Hu, H.; Larson, R. G. *Langmuir* **2005**, *21*, 3972.
(23) Hu, H.; Larson, R. G. *J. Phys. Chem. B* **2006**, *110*, 7090.
(24) Yu, H. Z.; Soolaman, D. M.; Rowe, A. W.; Banks, J. T. *ChemPhysChem* **2004**, *5*, 1035.
(25) Soolaman, D. M.; Yu, H. Z. *J. Phys. Chem. B* **2005**, *109*, 17967.
(26) Petsi, A. J.; Burganos, V. N. *Phys. Rev. E* **2005**, *72*, 047301.
(27) Petsi, A. J.; Burganos, V. N. *Phys. Rev. E* **2006**, *73*, 041201.
(28) Uno, K.; Hayashi, K.; Hayashi, T.; Ito, K.; Kitano, H. *Colloid Polym. Sci.* **1998**, *276*, 810.
(29) Fang, X.; Li, B.; Petersen, E.; Ji, Y.; Sokolov, J. C.; Rafailovich, M. H. *J. Phys. Chem. B* **2005**, *109*, 20554.
(30) Fang, X.; Li, B.; Sokolov, J. C.; Rafailovich, M. H.; Gewaily, D. *Appl. Phys. Lett.* **2005**, *87*, 094103.
(31) Fukai, J.; Ishizuka, H.; Sakai, Y.; Kaneda, M.; Morita, M.; Takanara, A. *Int. J. Heat Mass Transfer* **2006**, *49*, 3561.

10.1021/la0636309 CCC: $37.00
Published on Web 04/28/2007

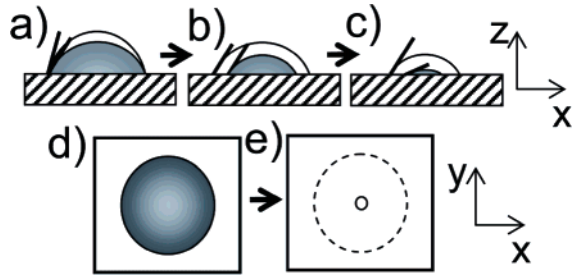

Figure 1. Schematic diagrams of the three distinct stages in the evaporation process of a droplet on a substrate and the formation of a drying stain: (a) constant contact area mode, (b) constant contact angle mode, (c) mixed mode, (d) initial droplet on a substrate (top view), and (e) drying stain on a substrate after droplet evaporation. The circular dashed line represents the initial contact line of the droplet, and the circular solid line represents the drying stain formed on a substrate after the evaporation of the droplet.

second stage is an unpinned phase in which the contact angle remains fixed (constant contact angle mode), and the third stage is an unpinned phase in which the contact angle decreases (mixed mode). Despite the experimental observation of these three stages of evaporation, the transition from the constant contact angle mode to the mixed mode has not yet been studied. In addition, understanding the morphology of drying stains with a diameter smaller than the initial droplet's diameter is important because of defect problems in immersion lithography.[32−34]

In this study, we used two different polymer films and various quantities of water droplets to explore the water droplet evaporation process and the morphology of drying stains. We investigated the changes in the weight and the shape of water droplets placed on polymer films by determining the contact angle, contact radius, and height at the center as a function of evaporation time with digital image analysis techniques. This study also obtained qualitative information about the microfluid flows inside the evaporating water droplets. Furthermore, the physical factors affecting the transitions between the evaporation modes are discussed, and the morphologies of the resulting stains on the polymer surfaces were investigated by comparing the theoretical direction of microfluid flow in the mixed mode with the experimental results.

Experimental Section

The polymer films were coated onto the native oxide layers of Si wafers (100). The Si wafers were cleaned by immersion in a H_2SO_4/H_2O_2 (7:3) solution for 20 min at 90 °C and then rinsed with deionized water. Two films with different hydrophobic properties (i.e., the initial contact angle, θ_i) were used: polymethylmethacrylate ($\theta_i = 67\pm 2°$, $M_w = 48\,500$ g/mol) as purchased from Polymer Source and poly(α-methyl styrene) ($\theta_i = 87 \pm 1°$, $M_w = 23\,000$ g/mol) as purchased from Pressure Chemicals. The films prepared from polymethylmethacrylate and poly(α-methyl styrene) are denoted PMMA and PAMS, respectively. PMMA and PAMS were prepared by spin coating from toluene solutions with concentrations of 1.3 and 1.2%, respectively, at a speed of 2000 rpm for about 60 s. To ensure that the samples had flat surfaces without solvent, the samples were annealed for 4 h at 40−50 °C above the bulk T_g under vacuum. PMMA and PAMS were found with atomic force microscopy (CP-II, Park Scientific Instruments) to have smooth, flat surfaces with 3 to 4 Å rms roughness. The thicknesses of annealed PMMA and PAMS were found to be about 44 ± 1 nm with ellipsometry (VASE, J. A. Woollam Co.).

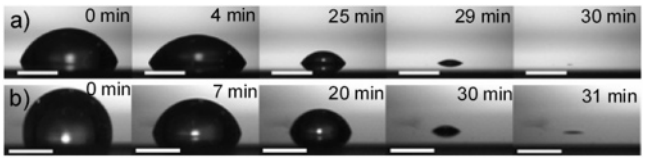

Figure 2. Images of water droplets during evaporation: (a) water droplet with initial weight of 2.19 mg on a PMMA surface and (b) water droplet with the initial weight of 2.14 mg on a PAMS surface. The inserted time in each image represents the time after the deposition of water droplets onto each surface. The scale bar in each image represents 1 mm.

To minimize the number of particles in the experimental environment, a transparent chamber with inside dimensions of 12 cm × 12.5 cm × 17 cm and a small hole on a microbalance with a sensitivity of ±10 μg (XS-105, Mettler Toledo) was used to observe the weight loss and shape changes of the water droplets on the polymer surfaces during evaporation. To ensure constant relative humidity and air flow during the experiments, dry nitrogen was purged at steady state at a constant rate (2 mL/min) inside the chamber. The constantly supplied nitrogen flow at a slow rate would prevent the saturation of water vapor and make sufficiently slow air convection inside the chamber because the rate of nitrogen flow is very low in contrast to the total volume of the chamber. The temperature and relative humidity in the chamber were approximately constant at 25−26 °C and 53 ± 1 %, respectively. Before the experiment, the balance pan was completely dried, and the balance was calibrated at room temperature to reach equilibrium with its environment. A quantity of deionized water (18.2 MΩ/cm, Millipore) in the range of 2.14−7.79 mg was deposited as a sessile drop from a micropipette onto the fresh polymer surfaces, and then the shape and weight loss of the water droplets were recorded every minute. While water droplets on the balance were evaporating, the weight of the water droplets slowly decreased, and the decrement in weight of the water droplets stopped after they completely evaporated without any balance drift problem. The dynamic contact angles on the polymer thin films were determined with the needle-syringe method by using a contact angle meter (Phoenix 300A, SEO) in separate measurements.

To observe the changes in the shapes of the water droplets during the evaporation process, fine images of the water droplets were acquired along an axis parallel to the surfaces of the thin films. A 100 mm macrolens and a digital camera (α-7D, Konica Minolta) with a 6 megapixels charge-coupled device were used with a light-emitting diode backlight. The lens was immediately adjusted to focus on the shape of the droplets when the water droplets were deposited onto each surface of the thin films. Then, images were recorded with an automatic interval of 1 min, and the weight on the balance was simultaneously manually recorded with the same interval. After all of the images had been acquired, precise digital image analysis was performed to determine the changes in the contact angle, radius, and height at the center of each water droplet on the basis of its reflection on polymer surfaces by using Photoshop 7.0 software. The determined radius and height were transformed into the real dimensions from the scale on the ruler that was intended to place the upside of deposited water droplets and was simultaneously taken into the images of water droplets. The compositions of the stains formed on the polymer surfaces after the evaporation of the water droplets were investigated with optical microscopy (OM) (Leitz) and energy-dispersive X-ray analysis (XL30SFEG, Phillips).

Results and Discussion

Figure 2 shows the sequences of images of evaporating water droplets with initial weights of 2.19 mg on a PMMA surface and 2.14 mg on a PAMS surface. As the evaporation proceeds, the volumes decrease within the sequence of the following three distinct stages: decreases in the contact angle (0−4 min on a PMMA surface, 0−7 min on a PAMS surface), in the contact

(32) Rothschild, M.; Bloomstein, T. M.; Kunz, R. R.; Liberman, V.; Switkes, M.; Palmacci, S. T.; Grenville, A. *J. Vac. Sci. Technol., B* **2004**, *22*, 2877.
(33) Gil, D.; Brunner, T. A.; Fonseca, C.; Seong, N.; Streefrerk, B.; Wagner, C.; Stavenga, M. *J. Vac. Sci. Technol., B* **2004**, *22*, 3431.
(34) Kusumoto, S.; Shima, M.; Wang, Y.; Shimokawa, T.; Sato, H.; Hieda, K. *Polym. Adv. Technol.* **2006**, *17*, 122.

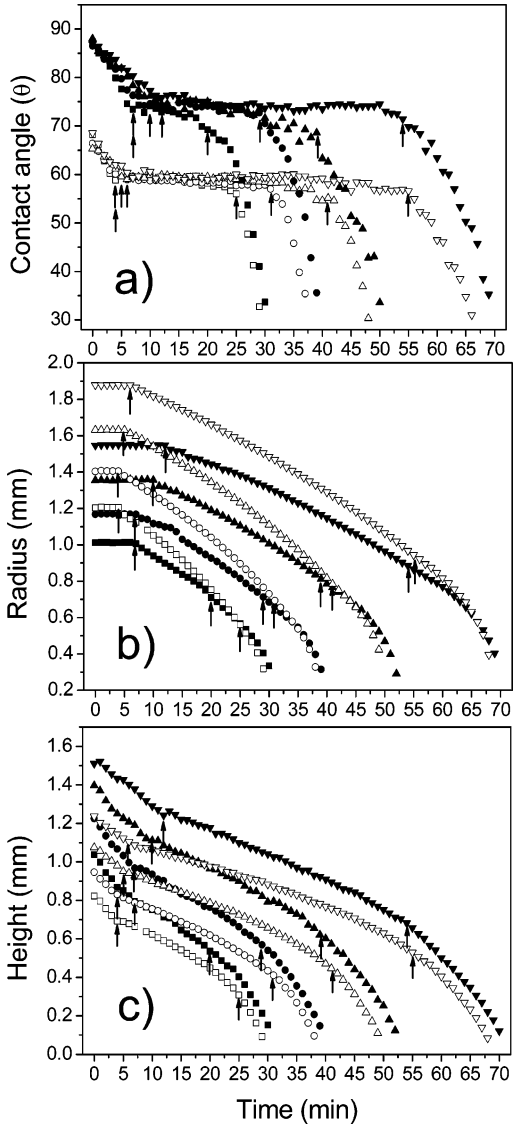

Figure 3. Shape changes of water droplets with initial weights of 2.19 mg (□), 3.18 mg (○), 5.04 mg (△), and 7.79 mg (▽) on PMMA surfaces and 2.14 mg (■), 2.96 mg (●), 4.91 mg (▲), and 7.33 mg (▼) on PAMS surfaces as a function of evaporation time: (a) contact angle, (b) contact radius, and (c) height at the center of the droplet. The arrows indicate the transition point of the evaporation mode.

area (4−25 min on a PMMA surface, 7−20 min on a PAMS surface), and in both the contact angle and area (25−30 min on a PMMA surface, 20−31 min on a PAMS surface) of water droplets.

Changes in the shapes of water droplets on the PMMA and PAMS surfaces are shown as a function of evaporation time for various initial quantities of water in Figure 3. Our results show that, regardless of the magnitude of the initial contact angle and the quantity of water in the water droplets, the evaporation invariably goes through three distinct stages. In the first stage, after a water droplet is deposited on the PMMA or PAMS surface, the contact radius of the water droplet is initially pinned, and the contact angle and the height of the water droplet at the center decrease linearly and simultaneously. Once the contact angle has attained its characteristic value on the PMMA or PAMS surface, the contact radius then starts to recede while the contact angle remains constant, with the decay rates of the height of the water droplet at its center drastically reduced. This second stage lasts for a long period of time during the evaporation. At the end of this stage, the contact angle suddenly decreases, and the third stage commences. At this point, the decay rates of the contact radius and of the height of the water droplet at the center gradually increase. Increasing the quantity of water increases the evaporation time, the contact radius, and the height of the water droplet, whereas the initial contact angle and the characteristic contact angle vary only with the surface properties and are independent of the quantity of water in the droplet.

These three distinct stages in the evaporation process are the constant contact area mode, the constant contact angle mode, and the mixed mode, as shown in Figure 1. Although the water droplets contain unexpected contaminants at very low concentrations in the initial stage, which we will discuss later in detail, the constant contact area mode and constant contact angle mode are explicitly observed. These results are consistent with previous studies that used pure water droplets.[24,25] Therefore, we conclude that the very low concentration of contaminants in water droplets would lead to slightly different contact angle values but would hardly affect these two modes.

The receding angles were determined from the characteristic contact angles of the water droplets on the PMMA and PAMS surfaces during the second stage and were found to be consistent with previously reported results.[8,24,25] The receding angles of the PMMA and PAMS surfaces were determined from the dynamic contact angle measurements by withdrawing the water droplet with the needle-syringe method and were found to be 57 ± 1 and 72 ± 1°respectively. The average contact angles in the constant contact angle mode for PMMA and PAMS surfaces are 60 ± 1 and 75 ± 1°, respectively. The difference between the receding angle determined with the needle-syringe method and that found during the evaporation process is caused by differences in the withdrawal rates of the water droplets.[8] Erbil et al. claimed that the drop evaporation method allows a minimum rate of liquid withdrawal that minimizes the linear rate of retreat effect on receding contact angle measurements. In constant contact area mode, the presence of surface roughness or chemical heterogeneities on the polymer surfaces results in contact angle hysteresis in which a pinned phase is maintained until the receding angle is attained. After the contact angle has reached the receding angle, which is the lowest possible contact angle and is determined by the thermodynamic states of the three phase (solid/liquid/vapor) boundaries, it becomes more favorable for the contact area of the water droplet to decrease than for the contact angle to decrease.

To check the accuracy of the data shown in Figure 3, we compared the weight of the water droplets as obtained with the microbalance with the volume calculated from eq 1 by assuming the spherical cap model

$$V(R, \theta) = \frac{\pi R^3(2 - 3\cos\theta + \cos^3\theta)}{3\sin^3\theta} \qquad (1)$$

where R is the contact radius and θ is the contact angle. As shown in Figure 4, the weight and volume losses of the water droplets vary nonlinearly with the evaporation time, and the calculated volume and measured weight are in agreement throughout the evaporation process within experimental error. This confirms that the acquired data are of high accuracy and that the water droplets all have the form of spherical caps on the PMMA and PAMS surfaces during evaporation. The applicability of the spherical cap model to the water droplets means that surface tension effects dominate gravity effects in this experimental range.

The weights of the water droplets at the transition points in the evaporation process were obtained from Figure 4 and are plotted against the initial weights of the water droplets, as shown

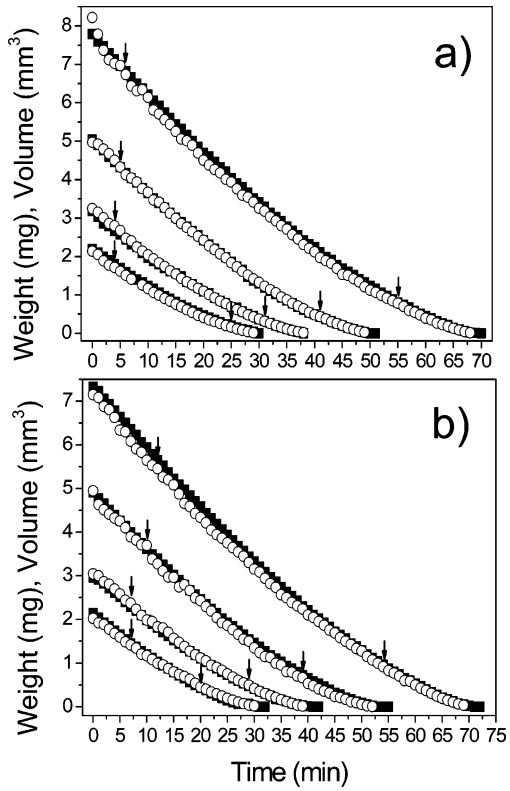

Figure 4. Volume (○) and weight (■) loss of water droplets as a function of evaporation time (a) on PMMA surfaces and (b) on PAMS surfaces. The arrows indicate the transition point of the evaporation mode in Figure 3.

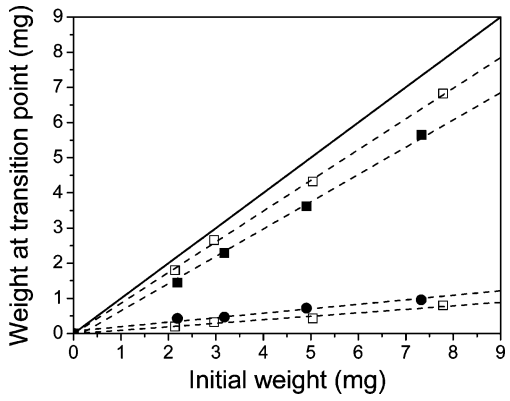

Figure 5. Critical weights of water droplets at the transition points in the evaporation process as a function of initial droplet weight: from constant contact area mode to constant contact angle mode on PMMA surfaces (□) and PAMS surfaces (■) and from constant contact angle mode to mixed mode on PMMA surfaces (○) and PAMS surfaces (●). The solid line represents the initial weight of the water droplet. The dashed lines are obtained by a linear fitting of the critical weights.

in Figure 5. Note that the weights at the transitions from the constant contact area mode to the constant contact angle mode and from the constant contact angle mode to the mixed mode vary linearly with the initial weight of the water droplets. From this experimental result, we conclude that the transitions in the evaporation process occur when certain portions of the water droplets have evaporated from the initial water droplets. As mentioned above, the first transition in the evaporation process is from the constant contact area mode to the constant contact angle mode and arises when the contact angle equals the receding angle. The slope of the variation of the weights of water droplets on PAMS surfaces with the initial weights of water droplets at the first transition is lower than that for PMMA surfaces. There are some ruptures with diameters on the scale of a few micrometers in the PAMS surfaces, which result from thermal instabilities due to the weak interaction between PAMS and the native oxide layer of Si.[35] These ruptures are not present on the PMMA surfaces. The larger nonuniformity provided by these ruptures on the PAMS surface is likely to cause a larger contact angle hysteresis than on the PMMA surfaces.

The behavior of the second transition, that between the constant contact angle mode and the mixed mode, is different from that of the first transition. The variations of the weights of water droplets on the PAMS and PMMA surfaces at the second transition with the initial weights of the water droplets are linear with only slightly different slopes. We conclude that a different physical factor is responsible for the transition from the constant contact angle mode to the mixed mode. The Marangoni instability is caused by the surface tension gradient in water droplets and is considered to be a significant factor leading to the mixed mode in the evaporation processes. One possible cause for the Marangoni instability is the dependence of surface tension on concentration and temperature. With a much low evaporation rate, the temperature effect on the surface tension is negligible from the evaporation of water droplets evolved in two distinct stages.[24,25] In the case of water droplets, therefore, the concentration is expected to be the dominant effect on the surface tension gradient compared to temperature. Although we used extremely pure water droplets, it is well known that water strongly attracts contaminants that are surface-active agents and so only rarely exhibits the surface tension of completely pure liquid water as in another study.[23] The water may already be contaminated from unexpected various sources such as the wall of a vial or the tip of a micropipette that was in contact with the water prior to the observation of the evaporation process. As the water droplets evaporate, the concentration of contaminants increases because of the continuous decrease in the water droplet volume. Then, at some critical concentration, the accidental emergence of a local gradient in the composition of the water droplets along the surface gives rise to a corresponding gradient in the surface tension.[36−38] A surface tension gradient in evaporating water droplets results in a contact angle that is lower than the receding angle in the constant contact angle mode.

There cannot be a static state in the water droplets in the presence of a surface tension gradient. To provide qualitative information about the direction of the microfluid flow inside an evaporating water droplet, the vertically averaged velocity ($v(r, t)$) of the microfluid was calculated from the experimental data. The vertically averaged velocity is useful as a quick measure of the inward or the outward flow of the microfluid during evaporation and can be expressed as shown in eq 2 by considering the conservation of fluid in an axisymmetric droplet, as shown in Figure 6[19]

$$v(r, t) = -\frac{1}{\rho r h}\int_0^r r\left(J_s(r, t)\sqrt{1+\left(\frac{\partial h}{\partial r}\right)^2} + \rho\frac{\partial h}{\partial t}\right)\mathrm{d}r \qquad (2)$$

where r is the radial distance from the center of the droplet, t is time, ρ is the density of the liquid, v is the vertically averaged velocity of the radial flow, h is the position of the air−liquid interface, and $J_s(r, t)$ is the rate of mass loss per unit surface area per unit time from the droplet by evaporation.

(35) Reiter, G. *Phys. Rev. Lett.* **1992**, *68*, 75.
(36) Aharon, I.; Shaw, B. D. *Phys. Fluids* **1996**, *8*, 1820.
(37) Ha, V. -M.; Lai, C.-L. *Int. J. Heat Mass Transfer* **2002**, *45*, 5143.
(38) Kaminskii, V. A.; Dil'man, V. V. *Theor. Found. Chem. Eng.* **2003**, *37*, 569.

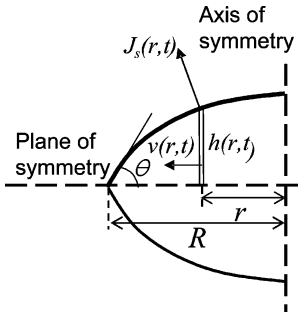

Figure 6. Axisymmetric droplet with the relevant parameters. The solid line represents the profile of the water droplet.

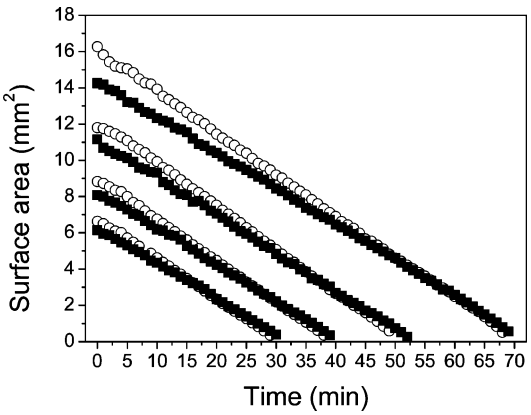

Figure 7. Change in surface area for water droplets as a function of evaporation time on PMMA surfaces (○) and on PAMS surfaces (■).

To simplify the integral in eq 2, the evaporation flux ($J_s(r, t)$) is assumed to be uniform over the surface area of the water droplet throughout the evaporation process. Then $J_s(r, t)$ in eq 2 can be rewritten as $J(t)$ (i.e., a time-dependent evaporation flux). This assumption is reasonable because the surface area of water droplets in the spherical cap model decreases linearly with evaporation time as shown in Figure 7 and as given by eq 3.

$$A(R, \theta) = \frac{2\pi R^2}{1 + \cos\theta} \qquad (0° \le \theta \le 90°) \tag{3}$$

We can then approximate the evaporation flux in the experimental data by using eq 4, which specifies $J(t)$ as the weight loss per unit time ($w_t - w_{t-1}$) per unit surface area of the water droplets (A_{t-1}).

$$J_s(r, t) = J(t) \cong \frac{w_{t-1} - w_t}{A_{t-1}} \tag{4}$$

The other parameter in the integral in eq 2 is the decay rate of the droplet profile ($\partial h(r, t)/\partial t$) as shown in eq 5, which is assumed to equal the decay rate of the height of the water droplet at the center ($\mathrm{d}h(0, t)/\mathrm{d}t$). This assumption is strictly applicable only to the constant contact angle mode. If we extend it to constant contact area mode and mixed mode, then the qualitative trend in microfluid flow can be obtained because the value of $|\partial h(r, t)/\partial t|$ is slightly lower than $|\mathrm{d}h(0, t)/\mathrm{d}t|$ and higher than $|J(t)|$ in almost the range of r.

$$0 \ge \frac{\partial h(r, t)}{\partial t} \ge \frac{\mathrm{d}h(0, t)}{\mathrm{d}t} \qquad (0 \le r \le R) \tag{5}$$

When the density (ρ) of the water droplet is 1, the vertically averaged velocity ($v(r, t)$) in eq 2 can be rewritten as eq 6:

$$v(r, t) = -\frac{r}{2h(r, t)}\left(J(t) + \frac{\mathrm{d}h(0, t)}{\mathrm{d}t}\right) \tag{6}$$

The height profile of the spherical cap ($h(r, t)$) can be calculated by using eq 7 from the spherical cap model:

$$h(r, t) = \sqrt{\left(\frac{h(0, t)^2 + R^2}{2h(0, t)}\right) - r^2} - \frac{R^2 - h(0, t)^2}{2h(0, t)} \tag{7}$$

The droplet profiles calculated with eq 7 are in good agreement with the observed droplet profiles in all of the experimental regions. There has been a debate in the literature as to whether the contact angle of a liquid on a solid is affected by droplet size or gravity. Some researchers have taken into account the effect of gravity in experiments.[39−41] In contrast, other researchers have suggested that the change in contact angle with droplet size is produced by hysteresis or line tension effects rather than by gravity.[42,43] We found that there is quite good agreement between observed droplet profiles and calculated droplet profiles even in a droplet with a weight of 7.79 mg. From this observation, we believe that the gravitational forces may affect droplets that are larger than 7.79 mg or that the distortion of the shape of the droplets not observed in our experiments may be due to other factors such as hysteresis or line tension effects.

The vertically averaged velocity ($v(r, t)$) was deduced from the experimental data given in Figure 3 by using eq 6. The derivative of the height of the droplet at the center with respect to the evaporation time ($\mathrm{d}h(0, t)/\mathrm{d}t$) was calculated by separating the evaporation process into the pinned state (constant contact area mode) and the depinned states (constant contact angle mode and mixed mode); the height of the droplets at the center does not change smoothly in the transition from the pinned state to the depinned state. In the case of the pinned state, the slope of the linear fit of the height of the droplet at the center was used as the derivative. In the case of the depinned states, the derivative ($\mathrm{d}h(0, t)/\mathrm{d}t$) was determined by using nonlinear curve fitting. The evaporation flux ($J(t)$) deduced from the experimental data given in Figures 4 and 7 by using eq 4 was also determined by using nonlinear curve fitting to reduce the scattering of the data produced by experimental uncertainty.

An example of the results of these calculations with eq 6 is given in Figure 8. We showed the variations with the normalized radius (r/R) of the normalized height profile of the droplet (calculated with eq 7) and the vertically averaged velocity of the microfluid inside the droplet (calculated with eq 6) for 2.19 mg of water on a PMMA surface. The height profile of the droplet changes with the evaporation mode, and the vertically averaged velocity of the microfluid in the radial direction of the droplet increases toward the edge of the droplet. In constant contact area mode and mixed mode, the normalized height profile gradually decreases. In constant contact angle mode, however, the normalized height profile does not change. Positive and negative values of the vertically averaged velocity indicate outward and inward flows of the microfluid, respectively. The divergence of the vertically averaged velocity at the edge of the droplet is caused by the approximation in eq 2. Therefore, this study can

(39) Pethica, B. A.; Pethica, P. J. C. *Proceedings of the 2nd International Congress of Surface Activity (London)*; Butterworths: London, 1957; Vol. 3, p 131.
(40) Leja, J.; Poling, G. W. *Proc. Int. Mineral Process. Congr.* **1960**, 325, paper no. 17, group III.
(41) Wada, T.; Fukumoto, T. J. *Jpn. Inst. Welding* **1968**, *37*, 845.
(42) Herzberg, W. J.; Marian, J. E. *J. Colloid Interface Sci.* **1970**, *33*, 161.
(43) Good, R. J.; Koo, M. N. *J. Colloid Interface Sci.* **1979**, *71*, 283.

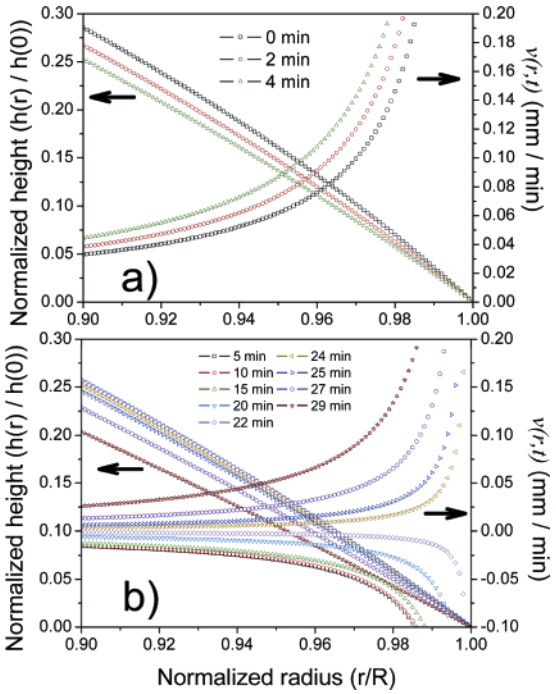

Figure 8. Normalized height profile ($h(r)/h(0)$) and vertically averaged velocity ($v(r, t)$) of microfluid against the normalized radius (r/R) in the range of 0.90−1.00 for water droplets on a PMMA surface with an initial weight of 2.19 mg (a) in constant contact area mode and (b) in constant contact area mode and mixed mode.

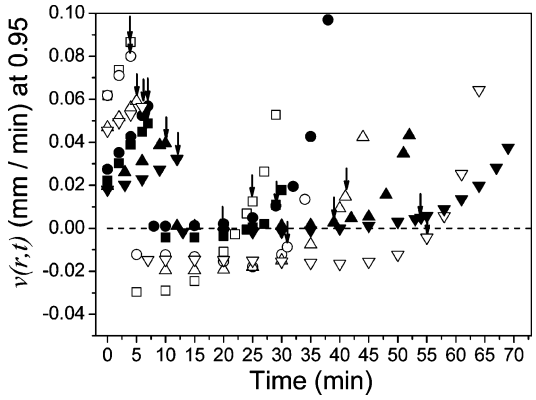

Figure 9. Vertically averaged velocity of a microfluid at a normalized radius of 0.95 for evaporating water droplets with initial weights of 2.19 mg (□), 3.18 mg (○), 5.04 mg (△), and 7.79 mg (▽) on PMMA surfaces and 2.14 mg (■), 2.96 mg (●), 4.91 mg (▲), and 7.33 mg (▼) on PAMS surfaces as a function of evaporation time. The arrows indicate the transition point of the evaporation mode in Figure 3.

provide only qualitative information about the microfluid flow inside evaporating water droplets.

Figure 9 shows the variation with evaporation time of the vertically averaged velocity of the microfluid at a normalized radius of 0.95 for evaporating water droplets on the PMMA and PAMS surfaces. The variation of the behavior of the microfluid with evaporation time is nearly independent of the initial quantity of water. The directions of the microfluid flow inside the water droplets on the PMMA and PAMS surfaces depend on the evaporation mode. In constant contact area mode, the vertically averaged velocity of the outward microfluid flow gradually increases. At the start of the constant contact angle mode, however, the direction of the microfluid flow changes from outward to inward or near zero, and the vertically averaged velocity is nearly constant during the constant contact angle mode. Furthermore, the magnitudes of the vertically averaged velocities of the

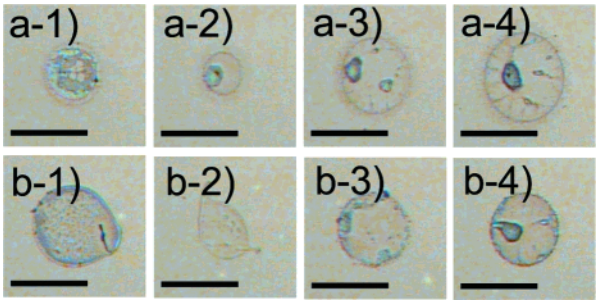

Figure 10. OM images of stains formed on polymer surfaces: (a-1−a-4) from water droplets with initial weights of 2.19, 3.18, 5.04, and 7.79 mg on PMMA surfaces, respectively, and (b-1−b-4) from water droplets with initial weights of 2.14, 2.96, 4.91, and 7.33 mg on PAMS surfaces, respectively. The scale bar in each image represents 0.5 mm.

microfluid in both constant contact area mode and constant contact angle mode are slightly higher on PMMA surfaces than on PAMS surfaces. These results are qualitatively consistent with previous results, which have shown that the directions of microfluid flows and the magnitudes of their vertically averaged velocities are dependent on the hydrophobic properties of surfaces.[26,27] In the mixed mode, which has not previously been described, the directions of microfluid flow gradually change from inward or near zero to outward, and the magnitude of the vertically averaged velocity gradually increases until the end of the evaporation process. The outward microfluid flow in the depinned state of a water droplet is due to the Marangoni instability, as mentioned above, which acts to suppress the local surface tension gradient.

The outward microfluid flow inside evaporating water droplets in the mixed mode results in ringlike stains on surfaces after evaporation.[18,19] We observed that circular stains form on both PMMA and PAMS surfaces after evaporation of the water droplets. As shown in Figure 10, the contaminants are concentrated at the perimeter of the stains, as expected for outward microfluid flows in mixed mode. In some cases, aggregates of contaminants form inside the stains. These aggregates were found to consist of a mixture of organic and ionic compounds that are thought to be surface-active agents, such as C, O, Na, Cl, and so on. The diameters of the stains were found to be near 0.5 mm and were independent of the hydrophobic properties of the surfaces and the variation of the initial weight of water droplets in the range of 2.14−7.79 mg.

Conclusions

We have demonstrated that there are three distinct stages in the evaporation of water droplets dominated by the surface tension effect, and we examined the variation of microfluid flow inside evaporating water droplets on two different hydrophobic polymer surfaces. The three distinct stages in the evaporation process are constant contact area mode, constant contact angle mode, and mixed mode. These modes occur regardless of variations in both the initial quantity of water in the water droplets and the hydrophobic properties of the polymer surfaces. The first and second transitions in the evaporation process are due to the attainment of the receding angle on the polymer surfaces and the Marangoni instability caused by the concentration gradients in the evaporating water droplets, respectively. As the water droplets evaporate, the behavior of the microfluid flow inside the water droplets was characterized by calculating the vertically averaged velocities from the experimental data. The directions and magnitudes of the vertically averaged velocities of the microfluid inside the evaporating droplets change, depending on the mode of evaporation and the hydrophobic properties of the surfaces,

regardless of the initial quantity of water. An outward microfluid flow is generated in mixed mode by the Marangoni instability, which acts to suppress the local surface tension gradient. However, there have been further studies on the aggregation of contaminants and of the observation that the stains on the polymer surfaces have nearly the same diameter (0.5 mm) regardless of the quantity of water required. The concentration of contaminants at the perimeter of the stains can be explained by outward microfluid flow in mixed mode. Thus, the formation of a pinned phase known as the coffee-stain phenomenon can be expected when there is a high concentration of contaminants and outward microfluid flow inside the evaporating water droplet during the final stage of evaporation. The nature of microfluid flow during the last stage of the evaporation process can provide an understanding of the morphology of drying stains after the evaporation of droplets on surfaces. This study advances our understanding of the defect morphologies produced by residual water droplets on photoresists in immersion lithography.

Acknowledgment. This work was supported by a Korea Science and Engineering Foundation (KOSEF) grant funded by the Korean government (MOST) (no. R01-2006-000-11221-0). We also appreciate the financial support and helpful advice from Samsung Electronics Co., Ltd.

LA0636309